Article

Discovery Medicine 2025; 37(200): 2032–2040
https://doi.org/10.24976/Discov.Med.202537200.174

Distribution Characteristics and Diagnostic Significance of Nestin in Stromal Components of Pleomorphic Adenoma of the Parotid Gland

Jian-xin Guo[1,2], Liang-cheng Tang[3], Fang Xu[3], Dao-chun Wang[2,*], Xiao-lan Han[1,*]

[1]Department of Stomatology, The First Affiliated Hospital of Anhui Medical University, 230022 Hefei, Anhui, China
[2]Department of Stomatology, The First People's Hospital of Chuzhou, 239000 Chuzhou, Anhui, China
[3]Department of Pathology, The First People's Hospital of Chuzhou, 239000 Chuzhou, Anhui, China
*Correspondence: wmm20231008@163.com (Dao-chun Wang); cheryl20231010@163.com (Xiao-lan Han)
Submitted: 7 July 2025 Revised: 7 August 2025 Accepted: 25 August 2025 Published: 20 September 2025

Background: Investigations into identifying novel immunohistochemical indicators are on the rise, aiming to elucidate tumor characteristics better. Therefore, this study examined the expression and distribution characteristics of nestin within the pleomorphic adenoma (PA) stromal component, and explored the potential mechanism underlying its formation, providing a comprehensive understanding of nestin's role as an immunohistochemical indicator.

Methods: This retrospective study included 51 patients diagnosed with PA of the parotid glands. The expression levels in the stromal component were assessed in patients' tissue specimens using immunostaining. Combined with computed tomography (CT) image analysis, the chi-square test, paired-sample *t*-test, Pearson's correlation coefficient, and principal component analysis (PCA) were used to explore the potential relationship between nestin expression characteristics and tumor parameters.

Results: Nestin was diffusely expressed in PA sections. The cellular arrangement in stromal components resulting from pseudopod-like protrusions appeared in "loose" and "reticular" patterns. These patterns were visualized through immunohistochemical staining, and the images were semi-quantitatively analyzed using ImageJ software. The two cellular arrangements showed statistical differences in the histomorphology of the stromal component, particularly between the "mucus-rich" and "cell-rich" ($p < 0.05$). CT imaging combined with Principal Component Analysis (PCA) revealed that the key factors affecting these two histomorphology types of stromal components were tumor area and CT value.

Conclusions: The formation of stromal components in PA is associated with changes in pseudopod-like cellular protrusions under different microenvironments. The tumor microenvironment and adjacent host tissue likely play a role in the development of PA. Furthermore, the "mucus-rich" structure tends to be more frequent in larger tumors. Nestin expression may contribute to maintaining the benign nature of PA, despite the stromal component being invasive. These results highlight the potential of nestin as an immunohistochemical marker, strongly associated with the formation and structural organization of stromal components.

Keywords: nestin; PA; stromal component; immunostaining; CT imaging

Introduction

The investigation of tumorigenic mechanisms has increasingly emphasized the importance of identifying immunohistochemical markers that reflect both the histopathological characteristics and the biological behavior of neoplastic tissues. Among these, intermediate filament proteins have gained significant attention due to their essential roles in maintaining cellular integrity and modulating dynamic processes such as proliferation, differentiation, and migration. Nestin, a class VI intermediate filament protein, was initially identified as a marker of neural stem cells but is now widely recognized for its expression in various progenitor cells and tumor cells. It has been associated with enhanced proliferative activity, elevated migratory potential, and greater invasiveness in malignant conditions, including glioblastomas, melanomas, and pancreatic carcinomas, indicating its role as a marker of cellular plasticity and structural remodeling during tumor progression [1–3].

Nestin, due to its crucial role in cytoskeletal dynamics and cell motility, emerges as a promising candidate for identifying dynamic cellular features within the myxoid component. Although previous studies have reported nestin expression in pleomorphic adenoma (PA) tissues [4], comprehensive investigations evaluating its distribution within the myxoid component and its association with specific morphological patterns remain limited. In routine histopathological practice, precisely identifying myxoid-rich areas can be challenging, especially when biopsy material is limited or when features overlap with other salivary gland neoplasms. Using nestin as a reliable immunohis-

tochemical marker could significantly enhance diagnostic precision, especially in cases where conventional histological assessment provides limited clarity. Furthermore, the capacity of nestin to highlight cytoplasmic protrusions and indicate cell motility may provide promising insights into tumor structure and progression.

Despite nestin's well-documented role in malignancies, its expression and functional significance in benign tumors remain relatively underexplored. Pleomorphic adenoma, the most frequent benign neoplasm of the salivary glands, particularly the parotid, demonstrates significant histological diversity. It includes epithelial, myoepithelial, and mesenchymal-like stromal elements, often presenting myxoid, chondroid, or hyaline areas. This complex architecture indicates the tumor's biological heterogeneity and may partially explain its locally invasive behavior and the risk of recurrence following surgical excision [5].

Within the histological spectrum of pleomorphic adenoma, the stromal component has garnered significant attention due to its distinct extracellular matrix (ECM) composition and its association with cellular pseudopod-like extensions, which may facilitate local infiltration. Research has suggested that pleomorphic adenomas exhibit proliferative characteristics resembling those of borderline tumors, given their potential for recurrence and rare malignant transformation [6]. However, these features do not recognize PA as a borderline tumor similar to those found in other organ systems. Moreover, the heterogeneity of the stromal components suggests that distinct biological mechanisms may drive the development of each tissue subtype, contributing to variable tumor behavior [7]. Specifically, the myxoid areas are suggested to create microenvironments permissive to cellular migration due to their distinct ECM composition, making the molecular characterization of these regions could provide valuable insights into the pathophysiology of pleomorphic adenoma [8].

Radiological imaging, especially computed tomography (CT), offers valuable preoperative insights into tumor size, location, density, and internal architecture. The relationship between histological composition and imaging characteristics is increasingly evident in salivary gland tumors. Particularly, myxoid-rich regions often appear as hypodense zones on CT scans, a finding due to their high mucopolysaccharide content.

Based on these observations, this study aimed to investigate the expression and spatial distribution of nestin within the stromal component of pleomorphic adenoma of the parotid gland. The analysis included immunohistochemical evaluation, quantification of nestin-positive areas, and histomorphological classification of stromal subtypes as either "mucus-rich" or "cell-rich". Furthermore, we examined the correlation between nestin expression patterns and CT imaging parameters. Using statistical approaches, including chi-square testing, paired sample *t*-tests, correlation analysis, and principal component analysis, we sought to determine whether nestin expression could serve as a marker for the structural organization and potential biological behavior in pleomorphic adenoma. The findings of this study may enhance our understanding of benign tumor behavior and support the diagnostic utility of nestin in clinical pathology.

Materials and Methods

Tissue Samples

This retrospective study recruited 51 patients diagnosed with PA of the parotid glands between 2017 and 2023. The study cohort comprised patients undergoing parotidectomy for the first time in The First People's Hospital of Chuzhou, China. Tissue samples collected from the patients were fixed in formalin and subsequently embedded in paraffin. All tissue specimens were archived in surgical blocks, which were preserved in the Department of Pathology. The inclusion criteria included no personal history of malignant tumors, no recent history of radiotherapy, and no tumor biopsy before surgery. For immunohistochemistry analysis, normal parotid gland tissues from the same patients were used as internal controls.

This study was approved by the Ethics Committee of The First People's Hospital of Chuzhou (CZ-Ethic-2023-006). Written informed consent was obtained from all patients before using their surgical specimens, and the study was conducted following the ethical principles outlined in the Declaration of Helsinki.

Immunohistochemical Staining

Formalin-fixed, paraffin-embedded PA tissue blocks were sectioned 4 µm-thick slices using a rotary microtome (Leica RM2235, Leica Biosystems, Nussloch, Germany). To assess nestin expression and its distribution within the stromal components, immunohistochemical staining was performed using a rabbit monoclonal anti-nestin antibody [clone EPR1301(2); Abcam, Cambridge, UK; Cat. no. ab176571] at a dilution of 1:500. Antigen retrieval was conducted by heating the tissue sections in citrate buffer (pH 6.0; ZSGB-BIO, Beijing, China; Cat. no. ZLI-9065) at 95 °C for 20 minutes, followed by blocking with 3% hydrogen peroxide (Solarbio, Beijing, China; Cat. no. H1056) for 10 minutes. Tissue sections underwent overnight incubation with the primary antibody at 4 °C, then were treated with a horseradish peroxidase (HRP)-conjugated goat anti-rabbit secondary antibody (Servicebio, Wuhan, China, Cat. no. GB23303) for 30 minutes at room temperature. Diaminobenzidine (DAB) substrate (ZSGB-BIO, Beijing, China; Cat. no. ZLI-9018) was applied for visualization, and hematoxylin (Solarbio, Cat. no. G1120) was used for nuclear counterstaining. Normal parotid tissue was used as a negative control, indicating no nestin expression. Positively stained cells, exhibiting brownish-yellow cytoplasmic or nuclear coloration, were examined under a

light microscope (Olympus BX53, Olympus Corporation, Tokyo, Japan) at 40× and 400× magnifications across five distinct stromal regions per section. Images were quantitatively analyzed using ImageJ software (version 1.53k; National Institutes of Health, Bethesda, MD, USA).

A cell was considered nestin-positive if its integrated optical density (IOD) was greater than zero. Stained was classified as diffuse if more than 30% of the field area was stained. The 30% threshold was selected as an optimal cut-off to minimize false positives from background staining (common at 20%) while avoiding missing weak staining that would occur with a 50% threshold. Furthermore, tumor stroma was classified based on myxoid tissue content: tissue sections with more than 50% myxoid tissue were categorized as the "mucus-rich" type, whereas those with less than 50% were classified as the "cell-rich" [9] type. For each tumor case, 1–2 representative adjacent sections were assessed to capture both central and peripheral areas of tumors. For evaluating the stromal component, pseudopod-like protrusions of nestin-positive cells were defined as having a "loose" arrangement if more than 50% of the cells were loosely connected (suggestive of cell dissociation), and as a "reticular" arrangement if less than 50% of the cells showed a loose arrangement (suggestive of cell connection).

CT Imaging and Data Analysis

CT scans were performed using a 2 × 64-slice CT scanner. The CT value and area of both the PA and the adjacent normal parotid gland tissue from the same patient were measured on axial images at the same anatomical level, ensuring a distance of at least 5 mm from the tumor margin to reduce partial volume effects. Representative regions were selected from contralateral or peripheral non-tumorous parotid areas, which were verified as morphologically normal based on radiological appearance. The measurements from these areas were then averaged for analysis.

Statistical Analyses

Statistical analyses were performed using Statistical Package for the Social Sciences (SPSS) (version 17.0; IBM Corp., Armonk, NY, USA) and R software (version 4.1.1; The R Foundation for Statistical Computing, Vienna, Austria). The Chi-square test was used to compare the proportion of pseudopod-like protrusions. A paired-sample *t*-test was used to compare the CT values between tumor tissues and adjacent normal tissues. The correlation between these variables was assessed using Pearson's correlation coefficient. Principal component analysis (PCA) was performed to evaluate the effects of PA parameters on histomorphological changes within stromal components and to identify the primary driving factors. A p-value of less than 0.05 was considered statistically significant.

Results

This study included 51 patients diagnosed with PA, comprising 20 males and 31 females, aged between 20 and 77 years, with body weights ranging from 46 to 90 kg. Among the 51 tumors, 38 were located in the superficial lobe and 13 in the deep lobe of the parotid gland, with tumor diameters ranging between 1 cm and 6 cm.

Expression and Distribution of Nestin in the Stromal Component

Immunostaining showed that nestin expression was reduced in normal parotid glands, however, it was consistently expressed in vascular endothelial cells, which were identifiable by their flat, elongated morphology and localization along the vascular lumina (Fig. 1). In contrast, in PA, nestin-positive stromal cells were localized within the myxoid matrix, demonstrating spindle- or stellate-shaped morphologies independent of vascular structures. Diffuse nestin expression was found across all 51 PA cases. In the myxoid tissues, nestin staining was more pronounced in the nuclear membrane, cytoplasm, and pseudopod-like protrusions of most nestin-positive cells, while a few cells lacked nuclear membrane staining. Additionally, these cellular protrusions varied in morphology and were predominantly observed in either a "loose" or "reticular" cellular arrangement (Fig. 2).

Histomorphological Differences of the Stromal Component

The stromal component PA can be grouped into two histomorphological types: "mucus-rich" and "cell-rich" [10], based on the characteristics and proportion of pseudopod-like protrusions. In pathological sections where the stromal component was predominant, the cellular protrusions were loosely arranged, with most cells remaining unconnected. Compared to the marginal region, the central areas had shorter cellular protrusions and larger intercellular distances (Fig. 2A–B). However, in some "mucus-rich" areas, certain pseudopod-like protrusions were interconnected, forming a "reticular" cellular arrangement due to distinctly oriented connections (Fig. 2D).

In pathological sections dominated by the "cell-rich" structure type, the cellular protrusions were more frequently interconnected, forming a "reticular" arrangement (Fig. 2C). Both the mucus-rich and cell-rich structural types can form reticular arrangements, with distinct cellular compartments and localized mucous foci (Fig. 2E,F). In contrast, in a few "cell-rich" sections, the protrusions appeared "loosely arranged", lacking interconnection (Fig. 2G–I). Additionally, in the mucinous mesenchyme area with a darker background, no nuclear membrane staining was observed (Fig. 2I). The Chi-square test verified that the distribution of these two cellular arrangements was statistically significantly different between the two histomorphological types of the myxoid structure ($p < 0.05$, Table 1).

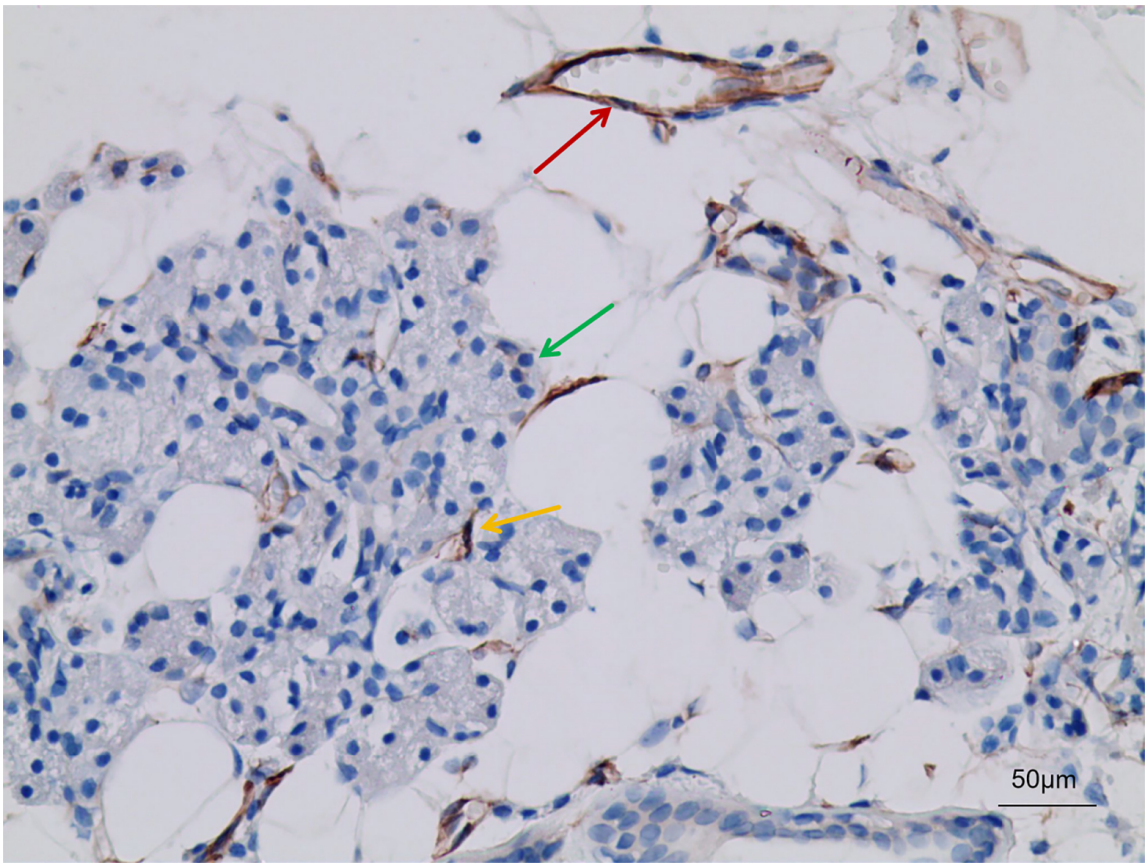

Fig. 1. Immunohistochemical staining for nestin in normal parotid gland tissue. Nestin-positive staining is observed in vascular endothelial cells (brown coloration), while acinar and ductal epithelial cells show no significant immunoreactivity. Red arrow: vascular endothelial cells showing nestin-positive staining (brown cytoplasmic signal along vessel walls); green arrow: acinar epithelial cells without nestin immunoreactivity; yellow arrow: myoepithelial cells with faint or no nestin expression. Hematoxylin counterstaining reveals nuclei in blue. The image represents a representative section from the control group. Magnification: 400×.

CT Value Differences Between Pleomorphic Adenoma and Normal Parotid Tissue

CT imaging revealed significant differences between PA tissues and adjacent normal parotid tissues across all 51 cases. In cell-rich PA (Fig. 3A), the lesions exhibited well-defined margins and relatively high CT attenuation values compared to surrounding normal tissue, likely due to the higher cellularity and fibrous stromal components. In contrast, mucus-rich PA (Fig. 3B) showed more poorly defined margins and lower CT attenuation values, consistent with their looser architecture and abundant mucinous stroma. In Fig. 3A,B, red arrows indicate the PA lesions, while red circles represent the adjacent normal parotid regions selected for CT value comparison.

A paired-sample *t*-test revealed that the mean CT attenuation values of PA tissues were significantly higher than those of the adjacent normal parotid tissues ($p < 0.05$; Fig. 3C), indicating a considerable difference in tissue density. Pearson's correlation coefficient was –0.48, indicating a moderate negative correlation between these two parameters (one-tailed $p = 3.45 \times 10^{-19}$; two-tailed $p = 6.90 \times 10^{-19}$).

Furthermore, to explore the associations between PA characteristics and histomorphological changes, we analyzed tumor parameters using Principal Component Analysis (PCA). The findings showed that "mucus-rich" PAs, identified based on high nestin expression in myxoid stromal regions, were primarily distributed along the Principal Component (PC1) axis, which was mainly driven by tumor size–related parameters, such as tumor diameter and tumor-to-parotid area ratio. In contrast, "cell-rich" PAs, with relatively lower nestin expression and more compact stromal arrangements, were distributed along the PC2 axis, which mainly indicated CT attenuation differences between the tumor and adjacent normal parotid tissue (Fig. 4A).

PC1 and PC2 accounted for 35.8% and 22.3% of the total variance, respectively, with tumor area and CT value being the primary contributors to PC1 and PC2 (Fig. 4B,C). These findings indicate that the nestin-defined stromal subtypes also exhibit distinct imaging features. Moreover, permutational multivariate analysis of variance (PERMANOVA) revealed significant differences in overall PA parameters between the "mucus-rich" and "cell-rich" groups ($p < 0.05$), indicating that these stromal subtypes

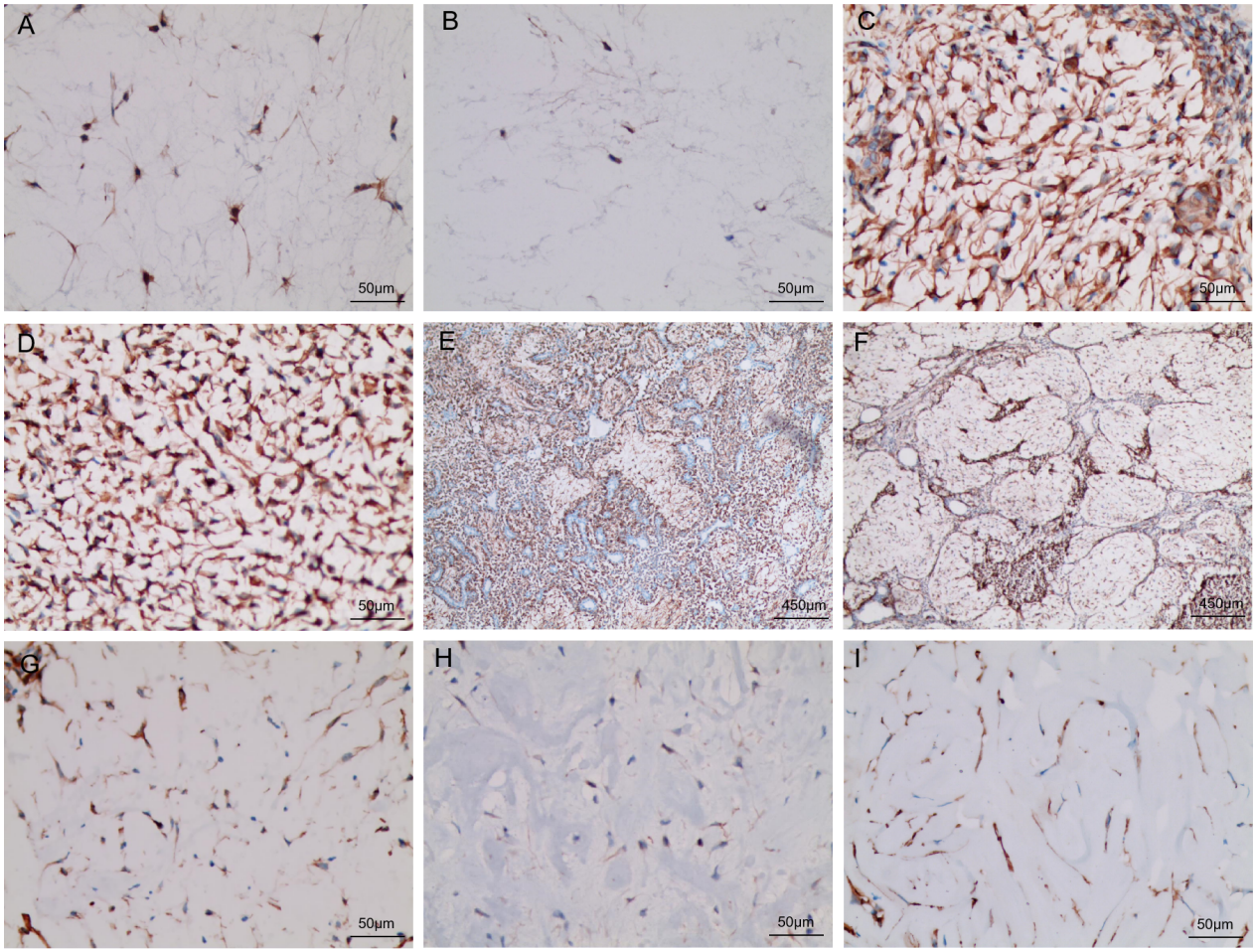

Fig. 2. Nestin expression in the stromal components of pleomorphic adenoma (PA). (A) The marginal region of the "mucus-rich" structure with a loose arrangement; (B) The central region of the "mucus-rich" structure with a loose arrangement; (C) The "cell-rich" structure with a reticular arrangement; (D) The "mucus-rich" structure with a reticular arrangement; (E) The fibrous septa or stromal compartments in the "cell-rich" structure; (F) The fibrous septa or stromal compartments in the "mucus-rich" structure; (G–I) the "cell-rich" structure with a loose arrangement in different myxoid mesenchyme backgrounds.

differ not only in histological nestin distribution but also in imaging and size-related features ($p < 0.05$, Fig. 4A).

A significant contribution of tumor diameter and the swelling-to-parotid area ratio would indicate a greater likelihood of mucinous histological patterns in tumors with larger diameters.

Discussion

Pleomorphic adenoma is a benign salivary gland tumor characterized by significant histological diversity, reflecting its complex biological behavior. Although PA lacks malignant histological features, the presence of elements such as cellular protrusions and matrix-rich zones suggests a degree of structural adaptability that may influence its growth and progression. In this study, we investigated the expression and spatial distribution of nestin, a type VI intermediate filament (IF) protein known to modulate cell migration, proliferation, and cytoskeletal remodeling, with a focus on its presence within the myxoid regions of PA. The study aimed to determine whether nestin expression correlates with distinct stromal morphologies—categorized as mucus-rich or cell-rich. Employing immunohistochemical staining combined with semi-quantitative image analysis, we identified two nestin-positive stromal patterns—loosely organized and reticularly organized protrusions. These arrangements were further assessed in relation to CT imaging features. These findings provide insights into nestin's role in stromal organization and its potential diagnostic value as an immunohistochemical marker in characterizing the histological complexity and behavioral diversity of PA.

Nestin is an Intermediate Filament (IF) protein primarily localized in the cytoplasm and nuclear lamina, playing a critical role in maintaining cytoskeletal organization [11]. In PA, nestin was highly expressed in the stromal component, a feature that is rarely noted in other common oral and maxillofacial tumors. This expression pattern suggests that

Table 1. The proportion of pseudopod-like protrusions in different histomorphology types of stromal component based on nestin immunostaining.

	Loosely arranged	Reticularly arranged	Total	χ^2 value	*p*-value
Mucus-rich	17	7	24		
Cell-rich	9	18	27	7.150	0.007
Total	26	25	51		
	Mucus-rich	Cell-rich	Total	χ^2 value	*p*-value
Loosely arranged	17	9	26		
Reticularly arranged	7	18	25	7.150	0.007
Total	24	27	51		

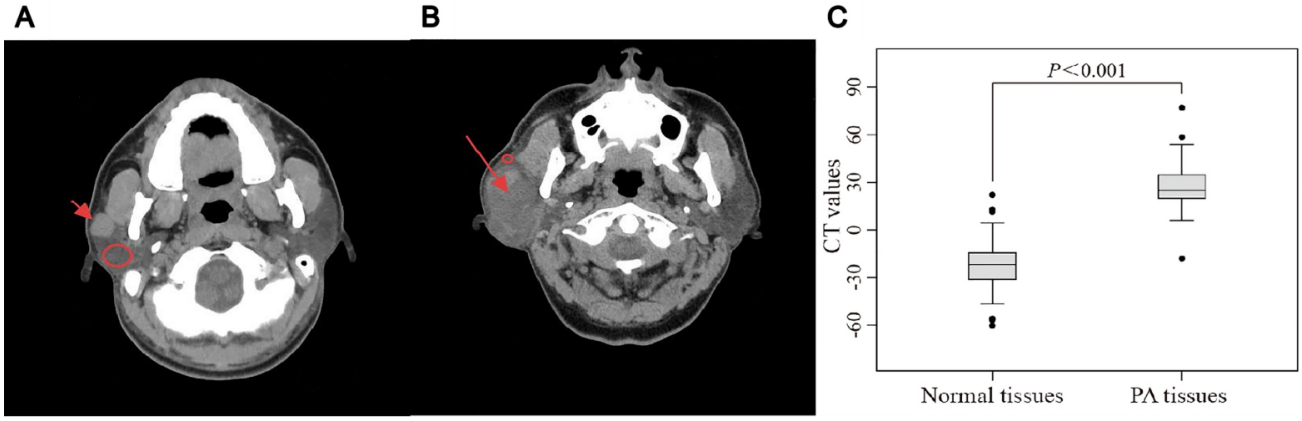

Fig. 3. Computed tomography (CT) imaging analysis of the "cell-rich" (A) and "mucus-rich" (B) types of PA in the included population (C). Red arrows indicate the location of the tumor, and red circles indicate the adjacent normal parotid tissue used for CT value comparison and the paired-sample *t*-test of differences in the CT values of PA and normal tissues (C).

nestin immunohistochemistry may aid in diagnosing PA, especially in biopsy specimens with limited myxoid tissue.

In "mucus-rich" PAs, nestin staining was consistently observed in both the nuclear membrane and cytoplasm. Most nestin-positive cells demonstrated "loosely arranged" protrusions of varying lengths, potentially reflecting differences in migratory capacity [12]. These morphological features only suggest possible differences in motility; however, functional studies are needed to validate this hypothesis. Despite cytoplasmic remodeling influenced by the mucinous stroma, persistent nuclear membrane staining may reflect structural stability that protects chromatin from mechanical stress during cell movement [13]. This structural resilience may help explain PA's benign nature, even in the presence of local stromal invasiveness. Conversely, fewer cells in mucus-rich PAs exhibited "reticularly arranged" protrusions, typically located within fibrous septa or dense stromal regions, suggesting limited motility consistent with the tumor's benign nature [14].

In "cell-rich" PAs, most nestin-positive cells exhibited reticular arrangements, forming cellular compartments with localized mucous foci. Although some "loosely arranged" protrusions were present, they appeared shorter and less frequent, suggesting reduced migratory potential. The presence of dense mucinous mesenchyme may mechanically constrain both stromal development and the formation of cellular protrusions [15,16]. In certain regions, irregular spindle-shaped cells with nuclear deformation were observed, often lacking nuclear membrane nestin staining. This may indicate nuclear damage resulting from the pressure exerted by the dense stroma, potentially serving as a histological indicator of mechanical stress or cellular strain [17–20]. Previous study has reported nestin expression in various neoplasms, including gliomas and pancreatic tumors, where it has been associated with stemness and increased invasiveness [21]. However, in benign salivary gland tumors like PA, nestin expression appears more localized to stromal structures rather than epithelial tumor components, suggesting a different biological role [2,22,23].

Radiological features also showed a close relationship with histomorphological subtypes. Principal component analysis indicated that "cell-rich" PAs demonstrated stronger associations with higher CT values, reflecting greater density compared to adjacent normal tissue. Conversely, "mucus-rich" PAs had lower CT values with less distinct contrast. Tumor diameter and tumor/parotid area ratio contributed more substantially to the "mucus-rich" group, consistent with their larger sizes and the higher proportion of loosely arranged nestin-positive cells. Together, these findings suggest that stromal organization in PA is in-

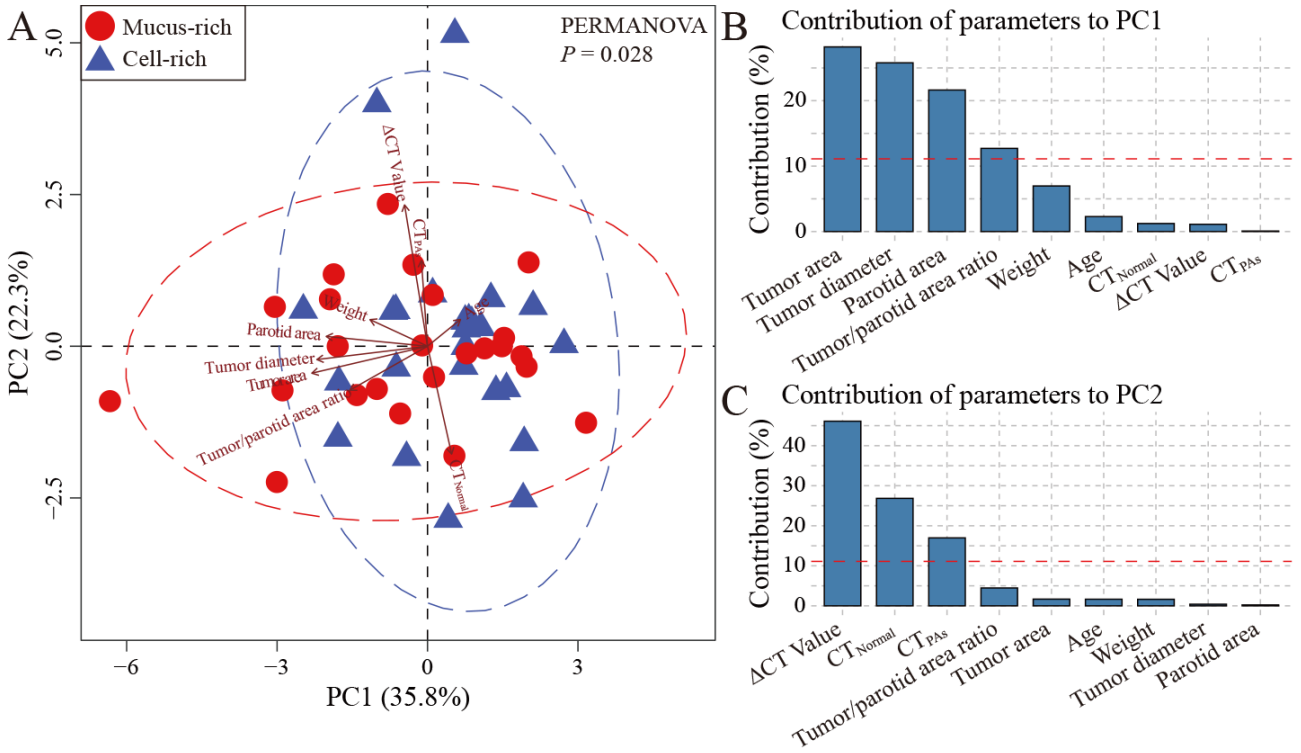

Fig. 4. Principal component analysis (PCA) of the effects of tumor parameters on the two histomorphology types of the stromal component of PA. (A) The results of PCA analysis showed that the mucinous patients were primarily distributed along the PC1 axis, while the cell-dense patients were mainly distributed along the PC2 axis, i.e., the PC1 axis (explaining 35.8% of the total variance) had a more pronounced effect on the mucinous patients, and the PC2 axis (explaining 22.3% of the total variance) had a more pronounced effect on the cell-dense patients. The results of permutation multivariate analysis of variance (PERMANOVA) showed a significant difference between mucinous and cell-dense patients ($p < 0.05$). (B) The predominant contributing factors of the PC1 axis were tumor area, tumor diameter, tumor area and tumor/gallbladder area ratio; (C) and the main contributing factors of the PC2 axis were the difference between normal and tumor tissue paired CT values, normal tissue CT values and tumor tissue CT values.

fluenced by both intrinsic tumor architecture and external mechanical or microenvironmental factors.

This study has several limitations which need to be acknowledged. Although the inclusion of 51 cases provided sufficient data for analysis, all samples were obtained from a single center, and the retrospective study design may have introduced selection bias. While immunohistochemistry and image-based quantification revealed distinct nestin expression patterns, the lack of complementary molecular assays, such as Western blotting or transcriptomic profiling, limited deeper mechanistic insights. The classification of stromal subtypes into "mucus-rich" and "cell-rich" types relied on semiquantitative morphological criteria; although supported statistically, this categorization would benefit from further validation employing digital pathology approaches or molecular markers. Moreover, the interpretation of CT imaging data was constrained by the absence of advanced imaging modalities, such as Magnetic Resonance Imaging (MRI), which could offer more comprehensive structural and functional evaluations. Future studies should incorporate larger, prospective multicenter cohorts, employ high-resolution imaging, and use multi-omics approaches to elucidate the regulatory pathways of nestin and its role in tumor-stroma dynamics.

Conclusions

Our findings suggest that nestin is not only diffusely expressed in the PA stromal components but also underscores distinct patterns of cellular protrusions—loosely arranged in mucus-rich areas and reticularly arranged in cell-rich regions—reflecting differences in cell motility and stromal remodeling. The stable localization of nestin at the nuclear membrane in mucus-rich zones may contribute to maintaining cytoskeletal integrity and safeguard chromosomal structural, thereby reinforcing the benign behavior of PA despite its local invasiveness. These findings support the potential of nestin as a marker for stromal differentiation and histological subtype classification in pleomorphic adenoma.

Availability of Data and Materials

Datasets used in this article are available from the corresponding authors on reasonable request.

Author Contributions

JXG: Conceptualization; Methodology; Data curation; Formal analysis; Writing - Original Draft; Writing - Review & Editing. LCT and FX: Formal analysis; Resources; Writing - Review & Editing. DCW: Conceptualization; Methodology; Funding acquisition; Project administration; Writing - Review & Editing. XLH: Conceptualization; Methodology; Supervision; Writing - Review & Editing. All authors read and approved the final version of the manuscript. All authors have participated sufficiently in the work and agreed to be accountable for all aspects of the work.

Ethics Approval and Consent to Participate

The study was approved by the Ethics Committee of The First People's Hospital of Chuzhou (CZ-Ethic-2023-006). Written informed consent was obtained from all patients before using their surgical specimens, and the study was conducted following the ethical principles outlined in the Declaration of Helsinki.

Acknowledgment

Not applicable.

Funding

This work was supported by the Scientific Research Project of the Anhui Provincial Health Commission (AHWJ2022c060).

Conflict of Interest

The authors declare no conflict of interest.

References

[1] Arrindell J, Desnues B. Vimentin: from a cytoskeletal protein to a critical modulator of immune response and a target for infection. Frontiers in Immunology. 2023; 14: 1224352. https://doi.org/10.3389/fimmu.2023.1224352.

[2] Pérez-Sayáns M, Chamorro-Petronacci CM, Baltazar F, Pires FR, Ínsua Á, Suárez-Quintanilla JA, *et al*. Nestin Expression Is Associated with Relapses in Head and Neck Lesions. Diagnostics (Basel, Switzerland). 2021; 11: 583. https://doi.org/10.3390/diagnostics11040583.

[3] Zhang Y, Wang J, Huang W, Cai J, Ba J, Wang Y, *et al*. Nuclear Nestin deficiency drives tumor senescence via lamin A/C-dependent nuclear deformation. Nature Communications. 2018; 9: 3613. https://doi.org/10.1038/s41467-018-05808-y.

[4] Dusart P, Fagerberg L, Perisic L, Civelek M, Struck E, Hedin U, *et al*. A systems-approach reveals human nestin is an endothelial-enriched, angiogenesis-independent intermediate filament protein. Scientific Reports. 2018; 8: 14668. https://doi.org/10.1038/s41598-018-32859-4.

[5] Piwowarczyk K, Bartkowiak E, Kosikowski P, Chou JTT, Wierzbicka M. Salivary Gland Pleomorphic Adenomas Presenting With Extremely Varied Clinical Courses. A Single Institution Case-Control Study. Frontiers in Oncology. 2021; 10: 600707. https://doi.org/10.3389/fonc.2020.600707.

[6] Choi SY, Choi J, Hwang I, Cho J, Ko YH, Jeong HS. Comparative Longitudinal Analysis of Malignant Transformation in Pleomorphic Adenoma and Recurrent Pleomorphic Adenoma. Journal of Clinical Medicine. 2022; 11: 1808. https://doi.org/10.3390/jcm11071808.

[7] Xu X, Xie J, Ling R, Ouyang S, Xiong G, Lu Y, *et al*. Single-cell transcriptomic analysis uncovers the origin and intratumoral heterogeneity of parotid pleomorphic adenoma. International Journal of Oral Science. 2023; 15: 38. https://doi.org/10.1038/s41368-023-00243-2.

[8] Chen W, Gu T, Chen Q, Qu C, Zhang C, Hu Y, *et al*. Extracellular matrix remodelling and stiffening contributes to tumorigenesis of salivary carcinoma ex pleomorphic adenoma–A study based on patient-derived organoids. Cell & Bioscience. 2023; 13: 122. https://doi.org/10.1186/s13578-023-01071-x.

[9] Urano M, Nakaguro M, Yamamoto Y, Hirai H, Tanigawa M, Saigusa N, *et al*. Diagnostic Significance of HRAS Mutations in Epithelial-Myoepithelial Carcinomas Exhibiting a Broad Histopathologic Spectrum. The American Journal of Surgical Pathology. 2019; 43: 984–994. https://doi.org/10.1097/PAS.0000000000001258.

[10] Cavalcante RB, Nonaka CFW, Rabenhorst SHB, da Costa Miguel MC, Pinto LP, de Souza LB. Pleomorphic adenoma and adenoid cystic carcinoma of salivary glands: E-cadherin immunoexpression and analysis of the CDH1 -160C/A polymorphism. Archives of Oral Biology. 2017; 73: 48–54. https://doi.org/10.1016/j.archoralbio.2016.09.005.

[11] Ndiaye AB, Koenderink GH, Shemesh M. Intermediate Filaments in Cellular Mechanoresponsiveness: Mediating Cytoskeletal Crosstalk From Membrane to Nucleus and Back. Frontiers in Cell and Developmental Biology. 2022; 10: 882037. https://doi.org/10.3389/fcell.2022.882037.

[12] Wang R, Khan S, Liao G, Wu Y, Tang DD. Nestin Modulates Airway Smooth Muscle Cell Migration by Affecting Spatial Rearrangement of Vimentin Network and Focal Adhesion Assembly. Cells. 2022; 11: 3047. https://doi.org/10.3390/cells11193047.

[13] Papadas A, Deb G, Cicala A, Officer A, Hope C, Pagenkopf A, *et al*. Stromal remodeling regulates dendritic cell abundance and activity in the tumor microenvironment. Cell Reports. 2022; 40: 111201. https://doi.org/10.1016/j.celrep.2022.111201.

[14] Scarini JF, de Lima-Souza RA, Lavareze L, Ribeiro de Assis MCF, Damas II, Altemani A, *et al*. Heterogeneity and versatility of the extracellular matrix during the transition from pleomorphic adenoma to carcinoma ex pleomorphic adenoma: cumulative findings from basic research and new insights. Frontiers in Oral Health. 2023; 4: 942604. https://doi.org/10.3389/froh.2023.942604.

[15] Xie K, Yang Y, Jiang H. Controlling Cellular Volume via Mechanical and Physical Properties of Substrate. Biophysical Journal. 2018; 114: 675–687. https://doi.org/10.1016/j.bpj.2017.11.3785.

[16] Jain RK, Martin JD, Stylianopoulos T. The role of mechanical forces in tumor growth and therapy. Annual Review of Biomedical Engineering. 2014; 16: 321–346. https://doi.org/10.1146/annurev-bioeng-071813-105259.

[17] Zhang Y, Fu Q, Sun W, Yue Q, He P, Niu D, *et al*. Mechanical forces in the tumor microenvironment: roles, pathways,

and therapeutic approaches. Journal of Translational Medicine. 2025; 23: 313. https://doi.org/10.1186/s12967-025-06306-8.

[18] Fischer T, Hayn A, Mierke CT. Effect of Nuclear Stiffness on Cell Mechanics and Migration of Human Breast Cancer Cells. Frontiers in Cell and Developmental Biology. 2020; 8: 393. https://doi.org/10.3389/fcell.2020.00393.

[19] Siddhartha R, Garg M. Interplay Between Extracellular Matrix Remodeling and Angiogenesis in Tumor Ecosystem. Molecular Cancer Therapeutics. 2023; 22: 291–305. https://doi.org/10.1158/1535-7163.MCT-22-0595.

[20] Han HM, Kim SY, Kim DH. Mechanotransduction for therapeutic approaches: Cellular aging and rejuvenation. APL Bioengineering. 2025; 9: 021502. https://doi.org/10.1063/5.0263236.

[21] Skálová A, Hyrcza MD, Leivo I. Update from the 5th Edition of the World Health Organization Classification of Head and Neck Tumors: Salivary Glands. Head and Neck Pathology. 2022; 16: 40–53. https://doi.org/10.1007/s12105-022-01420-1.

[22] Yanai H, Sato Y, Nagatsuka H, Yoshino T. Nestin is a wide-spectrum abluminal cell marker of salivary gland tumors. Pathology International. 2013; 63: 496–501. https://doi.org/10.1111/pin.12103.

[23] Yokoyama M, Katsumata-Kato O, Sakurai H, Ogawa H, Yoshigaki JF. Expression of a neural stem/progenitor cell marker nestin in salivary glands. MOJ Anat Physiol. 2017; 4: 291–294.